



Precise surface temperature measurements from 400 to 1200 K using the Pr:YAG phosphor

Dustin Witkowski¹ · David A. Rothamer¹

Received: 18 August 2021 / Accepted: 17 November 2021 / Published online: 30 November 2021
© The Author(s), under exclusive licence to Springer-Verlag GmbH Germany, part of Springer Nature 2021

Abstract

The thermographic phosphor Pr:YAG was investigated for lifetime-based surface temperature measurements using 4f–4f emission from its 3P_J states. A thin phosphor coating was applied to a fused silica substrate and placed in a tube furnace for diagnostic characterization. Lifetime measurements were performed from room temperature to 1200 K in 100-K increments. The emission lifetime was found to decrease continuously from 7 μ s at room temperature to 200 ns at 1200 K, making Pr:YAG a promising phosphor for applications involving fast transient phenomena. At each temperature, 100 single-shot measurements were acquired to evaluate phosphor performance. Single-shot temperature precision better than 2 K was measured from 400 to 1200 K. A methodology was developed for in-situ single-shot temperature precision estimates using weighted linear regression statistics. The precision predictions were compared to experimental results and agreement was generally within 1 K over the entire temperature range. The ability to precisely resolve temperature over large ranges in an applied environment was demonstrated using a propane torch to expose the phosphor-coated substrate to high heat fluxes. Measured temperature increased from room temperature to approximately 1150 K during the experimental duration, with estimated precision better than 4 K over the entire range

1 Introduction

There has recently been significant interest in the development of “temperature-swing” (T-swing) thermal barrier coatings (TBCs), characterized by low density and thermal conductivity, for reciprocating engines [1–5]. Employing these materials may allow surface temperatures to more closely track gas temperatures during combustion, reducing convective heat losses and improving thermodynamic efficiency [5, 6]. To date, engine performance results have been mixed, with some studies demonstrating benefits [2, 3, 7], while others show decreased performance [1, 8]. Multiple studies have identified potential adverse effects due to high porosity and increased surface roughness as reasons for the limited observed benefits [7, 9–11]. To better understand the impact of these new TBC materials on engine performance, in situ measurements of both surface temperature and heat flux are desired.

Phosphor surface thermometry is being actively developed for this purpose, both as a single-point and two-dimensional measurement technique [12–16]. Typically, thermographic phosphor particles are mixed with a binder and applied in a thin layer on the measurement surface. A laser is utilized to excite the phosphor particles which subsequently emit temperature-dependent radiation that can be utilized for thermometry. The focus of this work is on the lifetime thermometry approach, which has been used extensively to provide precise single-point temperature measurements for a range of different applications [17–21].

The temperature-swing of a TBC-coated piston during typical diesel engine operation may span a range from 450 K to over 1200 K [3], with temperatures changing as rapidly as a few kelvins every 20 μ s. To the authors’ knowledge, no phosphor composition has been identified that can precisely resolve measurements over this large of a temperature range with fast enough emission rates to maintain appropriate temporal resolution (see [21] for a list of many of the phosphors that have been tested in the literature). Fuhrmann et al. [17] has demonstrated high-speed measurements in an optically accessible engine using a $Mg_2TiO_4 : Mn^{4+}$ phosphor with suitably-fast emission rates. Unfortunately, its rapidly decreasing lifetime with temperature limits

✉ Dustin Witkowski
dwitkowski@wisc.edu

¹ University of Wisconsin-Madison, 1500 Engineering Dr., Madison, WI 53706, USA

precise measurements to approximately 500 K and below [21]. In addition, many measurements have been reported with Dy:YAG (and other Dy³⁺-based phosphors) from room temperature to at least 1700 K using both the lifetime and intensity ratio methods [21–23]. The slow characteristic emission rate of the Dy³⁺ ion (room temperature lifetime usually just below 1 ms) makes it unsuitable for resolving the rapid temperature swings expected during in-cylinder measurements when using the lifetime method for temperature determination.

Applications in highly transient environments, where single-shot precision cannot be measured directly, require estimation techniques to assess diagnostic performance and to reliably differentiate real temperature fluctuations from measurement noise. To date, this topic has received limited attention in the literature [16, 22]. Tsuchiya et al. [22] recently published a precision estimation technique based on non-linear regression statistics, although no comparison between statistical and measured shot-to-shot precision was performed.

The goal of the present work is twofold. First, trivalent praseodymium doped into yttrium aluminum garnet (Pr:YAG) is investigated as a candidate to resolve the potentially large temperature-swings for TBCs in reciprocating engine applications. Second, a method is developed that enables in-situ single-shot temperature precision estimates. This work extends previous work by Tsuchiya et al. [22] by comparing weighted linear regression statistical estimates directly to experimental results as a means of evaluating the suitability of statistical analysis for determining in-situ phosphor performance. Background on the lifetime thermometry technique is provided, including factors governing measurement precision and the method used to estimate the statistical single-shot signal-to-noise ratio from the lifetime measurements. The lifetime vs. temperature calibration is presented and the measured lifetime and temperature precision at each temperature are compared to predictions. Finally, results from a demonstration using a propane torch are presented to highlight the capability of the Pr:YAG phosphor to precisely resolve measurements over the relevant temperature range.

2 Background

2.1 Pr:YAG thermographic phosphor

The lifetime thermometry approach was employed to perform surface temperature measurements using the $^3P_J \rightarrow ^3H_4$ transition of Pr³⁺ doped into YAG (0.5% doping with Pr³⁺, Phosphor Technology Ltd., 1.8 μm median volume-weighted diameter based on manufacturer supplied particle volume probability distribution function). Pr:YAG has been identified as a

potential material for stable fluorescence-based thermometry utilizing the temperature dependence of its photoluminescence intensity [25]. It has also been used previously for gas temperature measurements [23, 24], but no applications employing the lifetime method have been reported in the literature to the authors' knowledge. Figure 1 displays the temperature-dependent normalized emission spectrum of this transition. The experimental setup for these measurements has been reported elsewhere [25]. The $^3P_J \rightarrow ^3H_4$ transition is narrow, centered at approximately 488 nm with a full-width half maximum (FWHM) of 3 nm at room temperature. With increasing temperature the peak very slightly red-shifts and preferentially broadens, with the FWHM increasing to 7 nm by 800 K.

2.2 Lifetime thermometry performance

The lifetime thermometry method utilizes the time decay of the phosphor emission to determine temperature. Upon excitation with a laser source, many phosphors undergo a nearly single exponential time decay of the luminescence signal [20]:

$$I_i = I_0 \exp\left(-\frac{t_i}{\tau}\right). \quad (1)$$

In Eq. (1), I_i is the intensity measured at time t_i and I_0 is the initial signal intensity directly after laser excitation assuming an excitation pulse duration which is short relative to the emission lifetime. The emission lifetime, τ , is a function of the phosphor's radiative emission probability ($A_R \equiv \text{Einstein}$

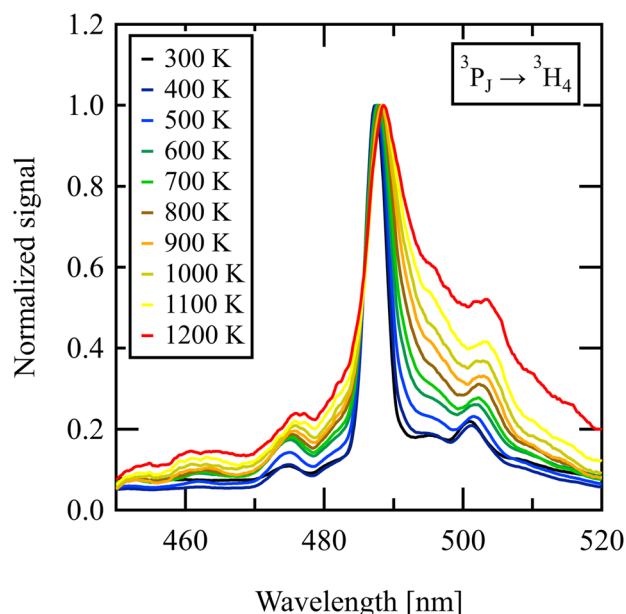


Fig. 1 Measured normalized emission spectrum as a function of temperature for the $^3P_J \rightarrow ^3H_4$ transition of Pr:YAG

A coefficient) and non-radiative transition probability (W_{NR}), that is

$$\tau = \frac{1}{A_R + W_{NR}}. \tag{2}$$

Whereas the radiative transition probability is usually considered to be temperature-independent, the nonradiative transition probability is a strongly increasing function of temperature. Once W_{NR} becomes similar in magnitude or greater than A_R , τ decreases significantly with increasing temperature. The resulting temperature-sensitivity of the emission lifetime can then be used for thermometry when calibrated appropriately.

The single-shot temperature precision (s_T , standard random uncertainty, i.e., the standard deviation of the sample distribution) for the lifetime method is dependent on the coefficient of variation for the lifetime measurement ($COV_\tau \equiv s_\tau/\tau$) and the fractional temperature sensitivity (ξ_T):

$$s_T = \frac{\partial T}{\partial \tau} s_\tau = \frac{s_\tau}{\tau} \frac{1}{\xi_T} = \frac{COV_\tau}{\xi_T}, \tag{3}$$

where

$$\xi_T = \frac{1}{\tau} \frac{\partial \tau}{\partial T} = \frac{\partial \ln \tau}{\partial T}, \tag{4}$$

and s_τ is the estimated single-shot lifetime measurement standard deviation. Measurement random uncertainty is minimized when two criteria are satisfied:

1. the lifetime is changing rapidly with temperature (i.e., high sensitivity), and
2. the relative random uncertainty in the lifetime measurement is small.

Temperature sensitivity can be determined from calibration experiments. Ideally, the measured lifetime is an intrinsic property of the phosphor and should directly translate to the application of interest. On the other hand, SNR_τ is more challenging to predict a priori. It not only depends on phosphor photophysical properties (absorption cross section, quantum yield, Einstein A coefficient), but is intimately linked to both the experimental setup details and fitting method used to determine the lifetime of each single-shot curve. Here, a technique is presented aimed at understanding measurement precision based on weighted linear regression statistics.

2.3 Weighted linear regression statistics

Linear regression fitting has been employed for the lifetime thermometry method extensively in the literature [16,

17, 26]. It is assumed that the phosphor decay curve can be adequately represented by Eq. (1). The equation is linearized by taking the natural logarithm, and the slope of $\ln I_i$ vs. t_i is used to determine the lifetime of the emission. The resulting linear regression model for the data is

$$\ln I_i = \ln I_0 - \frac{t_i}{\tau} + \varepsilon_i, \tag{5}$$

where ε_i is the error at time t_i between the predicted natural logarithm of the intensity and the measured intensity, i.e., $\widehat{\ln I_i} = \widehat{\ln I_0} - t_i/\widehat{\tau}$ (note that estimated/predicted quantities have a hat ^ over them). In general, ε_i is non-zero due to a combination of detector noise and fundamental limitations in the assumed fit form. The resulting weighted sum of squared errors is

$$S_w = \sum_{i=1}^N w_i \varepsilon_i^2 = \sum_{i=1}^N w_i (\ln I_i - \widehat{\ln I_i})^2, \tag{6}$$

where N is the number of data points used for fitting and w_i is the weighting factor for each point ($w_i = 1$ for un-weighted fits). The estimated lifetime of each single-shot curve is found by minimizing S_w with respect to $\ln I_0$ and $1/\tau$ [27], resulting in the following expression:

$$\frac{1}{\widehat{\tau}} = - \frac{\sum_{i=1}^N w_i (t_i - \bar{t}_w) (\ln I_i - \overline{\ln I_w})}{\sum_{i=1}^N w_i (t_i - \bar{t}_w)^2}. \tag{7}$$

In Eq. (7), the weighted mean of quantity x is defined as

$$\bar{x}_w = \frac{\sum_{i=1}^N w_i x_i}{\sum_{i=1}^N w_i}. \tag{8}$$

The random uncertainty in the estimated lifetime can be estimated from the statistical variance in the lifetime, calculated by taking the variance of Eq. (7) [27]:

$$s_{1/\widehat{\tau}}^2 = \frac{s_w^2}{\sum_{i=1}^N w_i (t_i - \bar{t}_w)^2}, \tag{9}$$

where

$$s_w^2 = \frac{S_w}{N - 2}. \tag{10}$$

The estimated coefficient of variation for the lifetime measurement is thus

$$COV_\tau = COV_{1/\tau} = \frac{s_{1/\widehat{\tau}}}{1/\widehat{\tau}}, \tag{11}$$

(see ‘‘Appendix 1’’ for a derivation of the equivalence of COV_τ and $COV_{1/\tau}$ in Eq. 11). Equation (9) can be used with Equation (11) for each single-shot time-resolved trace

to determine the variance in the fit for a given weighting-scheme. The next sections will compare the resulting precision estimates to experimental temperature precision, determined from 100 single-shot measurements taken from room temperature to 1200 K.

3 Experimental methods

3.1 Pr:YAG thermographic phosphor coating

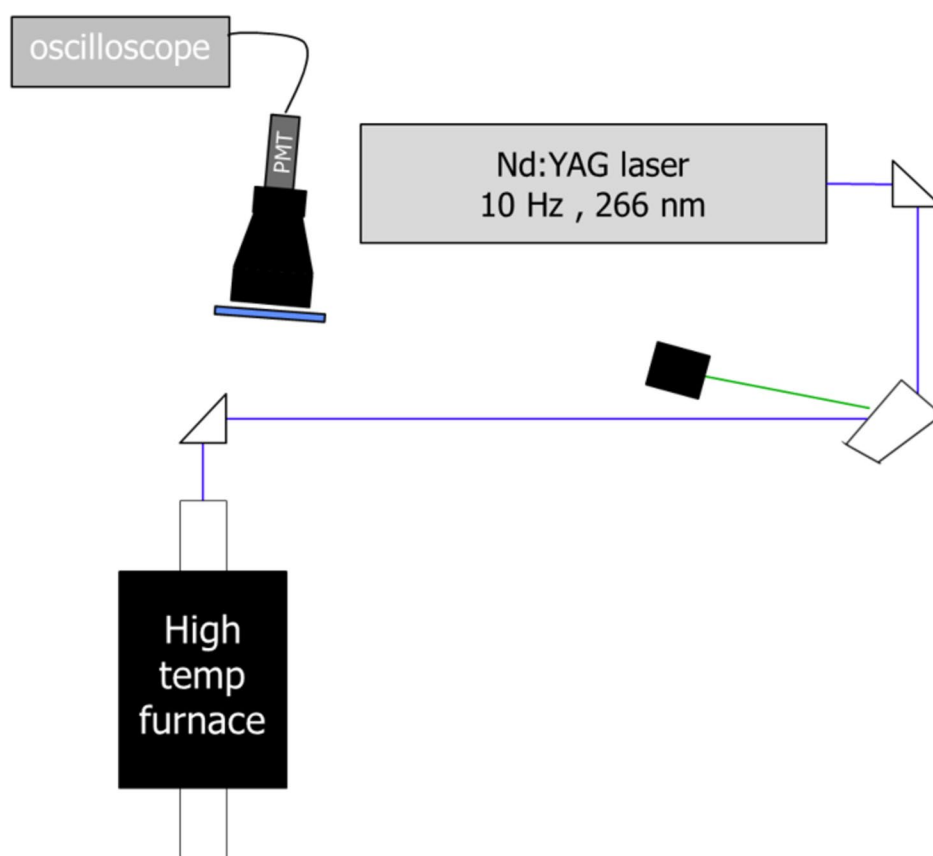
A phosphor coating was applied to the surface of a 25.4 mm diameter fused silica ground glass diffuser (Thorlabs DGUV10-220). The Pr:YAG phosphor particles were mixed with a high-temperature water-based binder liquid (ZYP Coatings, HPC binder) at a ratio of 1 g phosphor particles to 10 mL binder. The phosphor/binder mixture was brushed onto the substrate and then annealed in an oven at 200 °C for 3 h. No measurements of coating thickness were made, but based on previous measurements using a coating thickness gauge (Elcometer model 456) for similar coatings on aluminum substrates the thickness is estimated to be between 10 and 20 μm .

3.2 Furnace characterization

The experimental setup used for characterization of the Pr:YAG phosphor is shown in Fig. 2. Measurements were performed in a tube furnace (CM Furnaces, Rapid Temp Model 1720-12) from room temperature to 1200 K in 100-K increments. The phosphor coating was placed inside the furnace and excited with the 266-nm 4th-harmonic output of an Nd:YAG laser (Ekspla, NL-303D-10-SH/TH/FH) operated at 10 Hz, with an average pulse energy of 1.2 ± 0.2 mJ/pulse (2.5 ± 0.5 mJ/cm²). Emission was collected from 475 to 510 nm using a 500-nm shortpass filter (Edmund Optics 64663) and a 473-nm longpass filter (Semrock LP02-473RS-50). A 295-nm longpass filter (Schott WG-295) was also employed to reject laser scattering.

The time-resolved luminescence was measured using a photomultiplier tube (PMT) module (Hamamatsu, H-5783), with a rise time of 0.78 ns (based on manufacturer specifications). The built-in PMT amplifier was set to a control voltage of 0.62 V (corresponding to a current gain of 1.2E5 based on manufacturer's specifications) and stored on an oscilloscope (Teledyne Lecroy WaveSurfer 3034z, 350-MHz bandwidth, 8-bit resolution). The oscilloscope was operated at a sampling rate of 2 ns/point and a vertical scale of 200 mV/div. At each temperature, 100 single-shot measurements

Fig. 2 Experimental setup for the temperature-dependent time-resolved measurements



were acquired and processed to determine the mean and estimated standard deviation in the lifetime.

Luminescence lifetimes for each trace were calculated using the weighted linear least-squares regression defined by Eq. (7). Each single-shot measurement was first background subtracted using the average of the first 230 points prior to the laser excitation. Fitting began 100 ± 6 ns after the laser pulse to avoid any potential fast fluorescent interferences from the binder, substrate, or other background sources. Figure 3a displays examples of single-shot measurements beginning 100 ns after the laser pulse for temperatures of 600 K and 1200 K. At 1200 K a slow emission component is visible for intensities below 60 mV that is not as apparent at 600 K. This may be due to non-exponential behavior in the phosphor emission or could be a result of imperfect background subtraction of thermal emission at high temperatures. To avoid this artifact, lifetime fitting was chosen to end at a signal level of 80 mV for all measurements. This criteria was chosen rather than fitting utilizing an iterative window, as has been done previously [28]. The approach of Brübach et al. [28] was found to be prone to including the slow emission component at high temperatures, leading to poor fit results and significant biases in the temperature measurements.

In an effort to minimize COV_{τ} , the weighting for each point was set equal to the inverse of its' estimated variance [27] (see "Appendix 2"). Figure 3b provides examples of the fit results for single traces at three different temperatures.

The inclusion of weighting forces the fit to be best at early times, when signal intensities are high. Due to non-single exponential behavior early in the trace, especially at low temperatures (i.e., 400 K trace), this results in slightly worse agreement at later times. Even with this disagreement, it was found that the inclusion of weighting resulted in improved experimental COVs relative to unweighted fits, even at low temperatures.

3.3 Torch demonstration

Following furnace characterization and calibration of the Pr:YAG phosphor, a demonstration was performed utilizing a propane torch to expose the phosphor coating to high heat fluxes. The main purpose of the experiment was to demonstrate precise measurements over a large temperature range in a combustion environment. Figure 4 displays the experimental setup for the torch demonstration. Single-shot measurements were acquired directly on the oscilloscope for approximately 80 s at a rate of 2.2 traces every second (10,000 points were acquired per trace) until the measured temperature began to plateau. The torch position was manually adjusted such that the maximum temperature of the coating was approximately 1200 K (i.e., the maximum of the calibration range). The equipment and lifetime fitting details for these experiments were identical to that discussed in detail in Sect. 3.2.

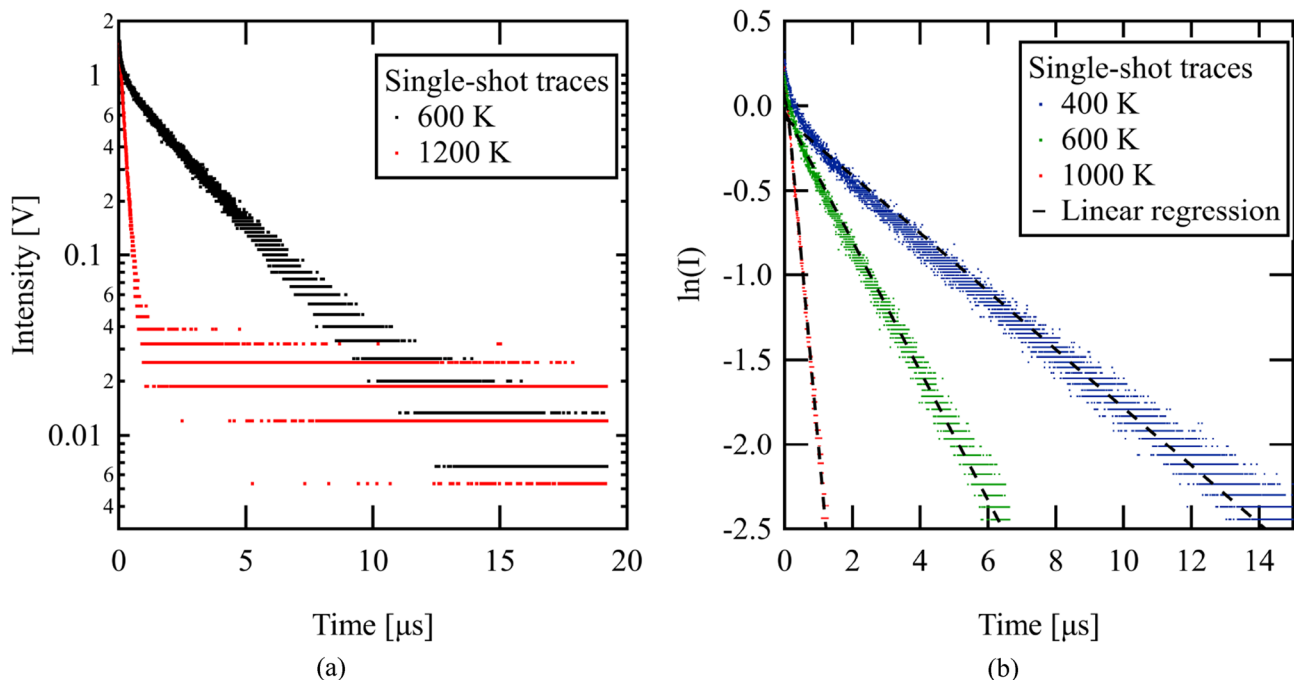
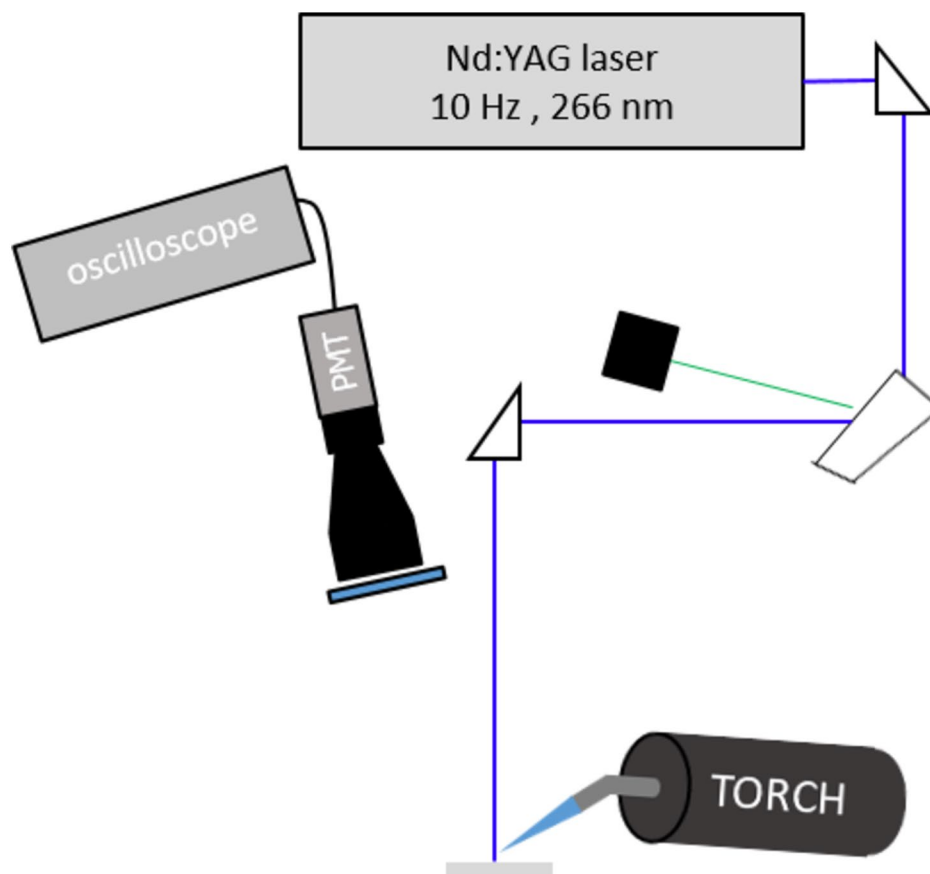


Fig. 3 **a** Measured single-shot intensity vs. time curves at 600 and 1200 K, **b** Lifetime fitting results for single-shot traces at 400, 600 and 1000 K

Fig. 4 Experimental setup for torch demonstration



4 Results

4.1 Lifetime calibration and temperature sensitivity

Figure 5a displays the average of 100 time-resolved measurements from room temperature to 1200 K. Measurements are cutoff at 80 mV to avoid the long lifetime component in the data, per Sect. 3.2 and Fig. 3a. With increasing temperature, the intensity decays more rapidly due to increasing nonradiative transition rates. At lower temperatures, there is a fast component that leads to non-single exponential behavior. Above 500 K, the fast component is less prevalent, and the data are better characterized by a single-exponential time decay. Beginning the lifetime fit 100 ns after the peak intensity allows the fit to be minimally impacted by the fast initial decay at temperatures above 400 K.

Figure 5b displays the measured lifetime vs. temperature (black symbols). At each temperature, the reported lifetime is the mean value of the 100 single-shot lifetime measurements. The lifetime is a continuously decreasing function of temperature, from approximately 7 μ s at room temperature down to 200 ns at 1200 K. This makes Pr:YAG phosphor a promising candidate for applications involving transient phenomena. On the other hand, the lifetime is still sufficiently long-lived to avoid

fluorescence interference (e.g., by delaying fitting until 100 ns after the laser pulse in this work) that can bias measurements in applied environments. The calibration used to translate lifetime into temperature is shown in Fig. 5b. The residual between the calibration fit and furnace temperature was less than 1% at all temperatures over this range, except at 500 K (1.3%).

The lifetime decreases approximately linearly on a logarithmic scale for temperatures above 400 K, implying a relatively constant fractional sensitivity (see Eq. 4). This is confirmed by directly calculating the fractional sensitivity using the lifetime vs. temperature calibration, as shown in Fig. 5b (blue line, right axis). By 500 K, the sensitivity is roughly 0.4%/K and remains between 0.4 and 0.45%/K from 500 to 1200 K. The magnitude of the sensitivity is moderate when considering that peak sensitivities for some phosphors are almost ten times higher [29].

Very high sensitivity allows for very precise temperature measurements; however, it is at the expense of a reduced temperature range. For the lifetime method, high sensitivity implies a rapidly decreasing lifetime. Therefore, as temperature increases fewer data points are acquired, reducing lifetime measurement precision and compromising the capability to precisely measure temperature over a large range. For the specific focus of this work (with temperature swings

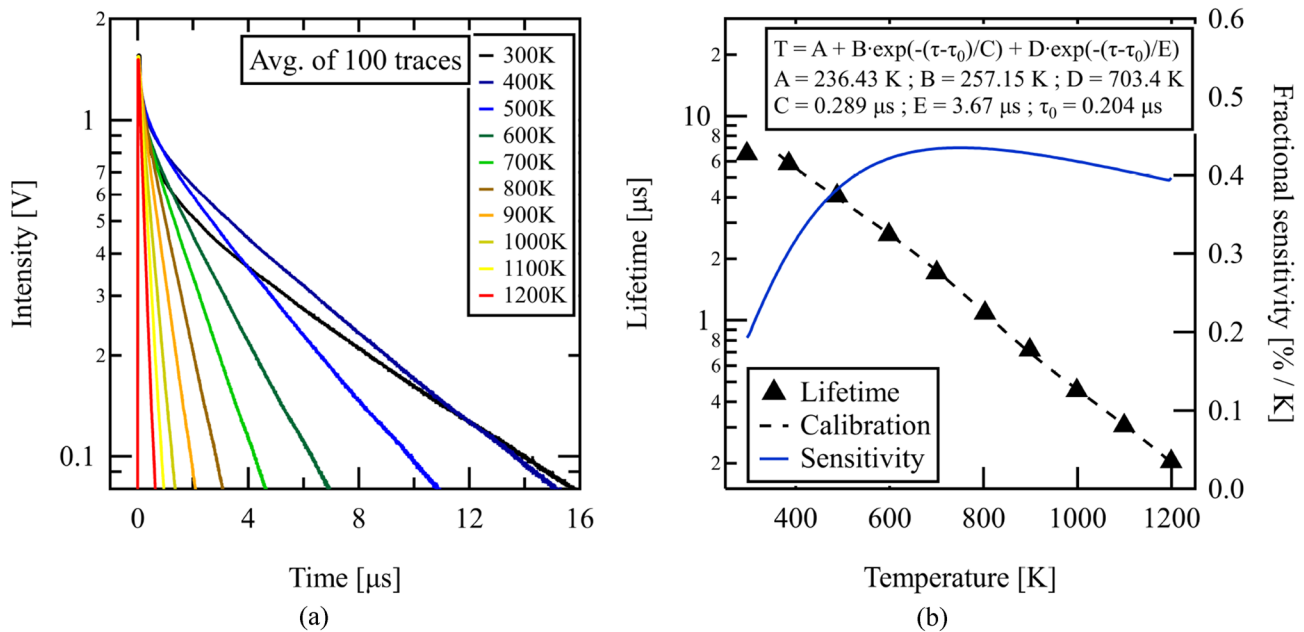


Fig. 5 **a** Average time-resolved curves for Pr:YAG from room temperature to 1200 K; **b** lifetime (black symbols, left axis) and fraction temperature sensitivity (blue line, right axis) vs. temperature

anticipated to be on the order of ~ 800 K), a moderate sensitivity phosphor such as Pr:YAG allows for precise measurements over the entire range of interest.

4.2 Temperature precision

Figure 6a displays the results of the 100 single-shot temperature measurements from 400 to 1200 K. Since each measurement set took roughly 45 s to complete (2.2 traces/s), a slow temperature drift was observed in the measurements of approximately 2–5 K from the first to the last data point at each temperature. The measurements reported were corrected for this by assuming a linear variation in time and applying a linear fit to determine the rate of variation needed for the correction.

The standard deviation of the 100 measurements at each temperature was calculated to determine the experimental temperature precision, and results are also shown in Fig. 6a. The experimental temperature precision (i.e., the random uncertainty s_T) is better than 2 K over the entire range. Correcting the measurements for temperature drift improved the measured precision on average by 0.14 K, with a maximum improvement of 0.5 K at 1100 K.

The measured precision is compared to the predicted temperature precision using Eq. (3) in Fig. 6b. On a relative basis the measured temperature precision is about a factor of two worse than predicted. From an absolute perspective, the agreement between measured and predicted precision is generally better than 1 K over the entire range. A linear

fit between measured and predicted precision is shown in Fig. 6b and will be used to estimate precision for the transient torch heating measurements. It is important to note that this linear relationship between experimental and statistical precision is specific to the experimental setup and conditions described in Sect. 3.2, and thus is not a general result. Measurements over a larger range of conditions (temperature, peak signal intensity, PMT gain, number of sampling points, oscilloscope resolution, etc.) could be employed to develop a more complete understanding of the relationship between experimental and predicted precision in the future.

4.3 Torch demonstration

Figure 7 displays the temperature vs. time of the Pr:YAG-coated fused silica substrate surface during the torch experiment. The torch was turned on approximately 7 s after data acquisition began (torch turn on corresponds to $t = 0$ s in the plot). Prior to the torch turning on, the phosphor diagnostic indicates a surface temperature of approximately 350 K. This is due to the poor calibration fit below 400 K, as such, measurements are only considered valid at temperatures above 400 K. Once the torch is turned on, there is a rapid initial increase in temperature. The measured surface temperature plateaus at 1150 K approximately 50 s after the torch was turned on. The single-shot estimated temperature precision (red dots) based on the relationship reported in Sect. 4.2, is between 1 K (450 K) and 4 K (1150 K) over the entire range. In comparison, the single-shot temperature

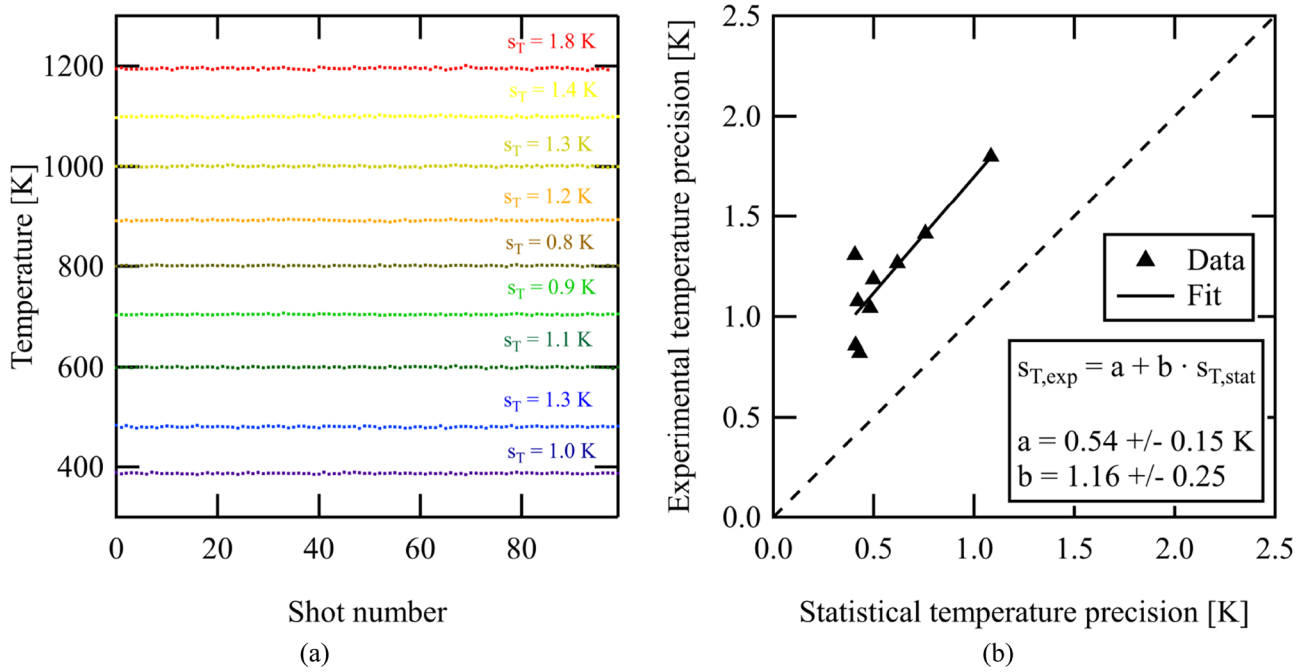


Fig. 6 a 100 single-shot temperature measurements from 400 to 1200 K; b experimental vs. statistically predicted temperature precision

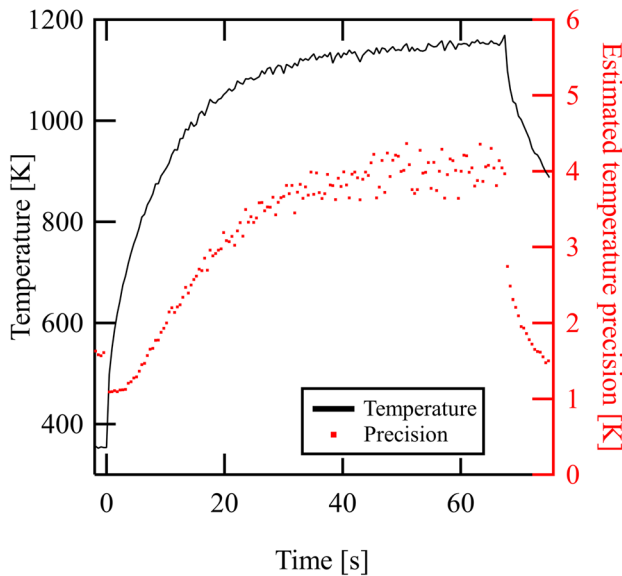


Fig. 7 Measured temperature (black) and estimate precision (red dots, right axis) vs. time for torch experiment

standard deviation over the last 20 data points ($T \approx 1150$ K) prior to the torch being turned off, when the temperature has essentially stopped changing, was 4.1 K.

5 Conclusions

This work investigated the Pr:YAG phosphor as a candidate for surface temperature measurement applications requiring large temperature ranges and fast temporal resolution. From 400 to 1200 K the measured lifetime decreased from approximately $6 \mu\text{s}$ to 200 ns. The lifetime dependence on temperature was used for thermometry, and the performance of the phosphor was evaluated in a tube furnace. Single-shot temperature precision of 2 K or better was measured over the entire calibration range from 400 to 1200 K. Measurements were compared to statistical predictions of temperature precision, and agreement was generally within 1 K over the entire range. Finally, measurements were performed with a propane torch to expose the phosphor-coated substrate to a high heat flux. Measured temperature increased from room temperature to approximately 1150 K during the experimental duration, with estimated precision better than 4 K over the entire range.

Appendix 1: Equivalence of $\frac{\tau}{s_\tau}$ and $\frac{1/\tau}{s_{1/\tau}}$

The equivalence between $\frac{\tau}{s_\tau}$ and $\frac{1/\tau}{s_{1/\tau}}$, can be derived by starting with the expression for temperature precision. This can be written both as function of τ

$$s_T^2 = \left(\frac{\partial T}{\partial \tau}\right)^2 s_\tau^2 = \text{COV}_\tau^2 \frac{\tau^2}{\left(\frac{\partial \tau}{\partial T}\right)^2}, \tag{12}$$

and as a function of $1/\tau$.

$$s_T^2 = \left(\frac{\partial T}{\partial(1/\tau)}\right)^2 s_{1/\tau}^2 = \text{COV}_{1/\tau}^2 \frac{1/\tau^2}{\left(\frac{\partial(1/\tau)}{\partial T}\right)^2}, \tag{13}$$

where $\text{COV}_\tau = s_\tau/\tau$ and $\text{COV}_{1/\tau} = s_{1/\tau}/(1/\tau)$ were previously defined. Next, $\frac{\partial(1/\tau)}{\partial T}$ can be written explicitly in terms of $\frac{\partial \tau}{\partial T}$ as

$$\frac{\partial(1/\tau)}{\partial T} = \frac{\partial(1/\tau)}{\partial \tau} \frac{\partial \tau}{\partial T} = -\frac{1}{\tau^2} \frac{\partial \tau}{\partial T}. \tag{14}$$

Plugging (14) into (13), we get

$$s_T^2 = \text{COV}_{1/\tau}^2 \frac{\tau^2}{\left(\frac{\partial \tau}{\partial T}\right)^2}. \tag{15}$$

Since (12) and (15) are equal, COV_τ is equal to $\text{COV}_{1/\tau}$.

Appendix 2: Linear regression weighting

The variance in the linear regression fit, given by Eq. (6), can be re-written as

$$S_w = \sum_{i=1}^N w_i \left(\ln \frac{I_i}{\hat{I}_i}\right)^2 = \sum_{i=1}^N w_i \left(\ln \left(\frac{I_i - \hat{I}_i}{\hat{I}_i} + 1\right)\right)^2. \tag{16}$$

To minimize the variance in the fit, the weighting was set equal to the inverse of the un-weighted fit variance [27].

$$w_i = \left(\ln \left(\frac{I_i - \hat{I}_i}{\hat{I}_i} + 1\right)\right)^{-2} \approx \left(\ln \left(\frac{1}{\text{SNR}_{i,p}} + 1\right)\right)^{-2}, \tag{17}$$

$\text{SNR}_{i,p}$ is the predicted signal-to-noise ratio in the detector at time i , and all other terms have been defined in the main text. $\text{SNR}_{i,p}$ can be estimated based on PMT noise characteristics [30] and oscilloscope vertical resolution.

$$\text{SNR}_{i,p} = \left(\frac{K_1}{I_i} + \frac{K_2}{I_i^2}\right)^{-1/2}, \tag{18}$$

$$K_1 = a^2 2e \Delta f G R_f, \tag{19}$$

$$K_2 = 4kT \Delta f R_f + a^2 2e i_{cd} \Delta f G^2 R_f^2 \eta + \left(\frac{V_{\text{range}}}{2^N \sqrt{12}}\right)^2. \tag{20}$$

Table 1 Estimated photomultiplier tube and oscilloscope operating parameters

Symbol	Definition	Value	Units
a	Factor for statistical gain fluctuation	1.4	[-]
e	Electron charge	1.6E-19	[C]
Δf	Bandwidth of amplifier-readout system	5E+8	[Hz]
G	Current gain of PMT	1.2E+5	[-]
R_f	Load resistor	50	[Ohms]
k	Boltzmann constant	1.38E-23	[J/K]
T	Resistor temperature	300	[K]
i_{cd}	Photocathode dark current	2E-10	[A]
η	Collection efficiency of first PMT dynode	1	[-]
V_{range}	Oscilloscope voltage range	2	[V]
N	Number of oscilloscope bits	8	[]

All terms are defined in Table 1, and values used are based on manufacturer specifications or estimated from literature [30].

Acknowledgements Funding for this work was provided by Caterpillar Inc.

References

1. S. Caputo, F. Millo, G. Boccardo, A. Piano, G. Cifali, F.C. Pesce, Numerical and experimental investigation of a piston thermal barrier coating for an automotive diesel engine application. *Appl. Therm. Eng.* **162**, 114233 (2019)
2. T. Powell, R. O'Donnell, M. Hoffman, Z. Filipi, E.H. Jordan, R. Kumar, N.J. Killingsworth, Experimental investigation of the relationship between thermal barrier coating structured porosity and homogeneous charge compression ignition engine combustion. *Int. J. Engine Res.* **2**, 1468087419843752 (2019)
3. M. Andrie, S. Kokjohn, S. Paliwal, L.S. Kamo, A. Kamo, D. Procknow, Low heat capacitance thermal barrier coatings for internal combustion engines, Report 0148-7191, SAE Technical Paper (2019)
4. N. Uchida, A review of thermal barrier coatings for improvement in thermal efficiency of both gasoline and diesel reciprocating engines. *Int. J. Eng. Res.* **20**, 1468087420978016 (2020)
5. J.C. Saputo, G.M. Smith, H. Lee, S. Sampath, E. Gingrich, M. Tess, Thermal swing evaluation of thermal barrier coatings for diesel engines. *J. Therm. Spray Technol.* **20**, 1–15 (2020)
6. N. Killingsworth, T. Powell, R. O'Donnell, Z. Filipi, M. Hoffman, Modeling the effect of thermal barrier coatings on HCCI engine combustion using CFD simulations with conjugate heat transfer (2019-04-02 2019). <https://doi.org/10.4271/2019-01-0956>
7. E. Gingrich, M. Tess, V. Korivi, P. Schihl, J. Saputo, G.M. Smith, S. Sampath, J. Ghandhi, The impact of piston thermal barrier coating roughness on high-load diesel operation. *Int. J. Engine Res.* **20**, 1468087419893487 (2019)
8. P. Andruskiewicz, P. Najt, R. Durrett, R. Payri, Assessing the capability of conventional in-cylinder insulation materials in achieving temperature swing engine performance benefits. *Int. J. Engine Res.* **19**(6), 599–612 (2018)

9. Z. Filipi, M. Hoffman, R. O'Donnell, T. Powell, E. Jordan, R. Kumar, Enhancing the efficiency benefit of thermal barrier coatings for homogeneous charge compression ignition engines through application of a low-k oxide. *Int. J. Engine Res.* **20**, 1468087420918406 (2020)
10. J. Somhorst, W. Uczak De Goes, M. Oevermann, M. Bovo, Experimental evaluation of novel thermal barrier coatings in a single cylinder light duty diesel engine (2019-09-09 2019)
11. Y. Wakisaka, M. Inayoshi, K. Fukui, H. Kosaka, Y. Hotta, A. Kawaguchi, N. Takada, Reduction of heat loss and improvement of thermal efficiency by application of "temperature swing" insulation to direct-injection diesel engines. *SAE Int. J. Engines* **9**(3), 1449–1459 (2016)
12. Q. Fouliard, S. Haldar, R. Ghosh, S. Raghavan, Modeling luminescence behavior for phosphor thermometry applied to doped thermal barrier coating configurations. *Appl. Opt.* **58**(13), D68–D75 (2019)
13. Q. Fouliard, J. Hernandez, B. Heeg, R. Ghosh, S. Raghavan, Phosphor thermometry instrumentation for synchronized acquisition of luminescence lifetime decay and intensity on thermal barrier coatings. *Meas. Sci. Technol.* **31**(5), 054007 (2020)
14. J.I. Eldridge, A.C. Wroblewski, D. Zhu, M.D. Cuy, D.E. Wolfe, K. Irsee, Temperature mapping above and below air film-cooled thermal barrier coatings using phosphor thermometry
15. C. Binder, H. Feuk, M. Richter, Phosphor thermometry for in-cylinder surface temperature measurements in diesel engines. *J. Luminescence* **20**, 117415 (2020)
16. N. Fuhrmann, C. Litterscheid, C.P. Ding, J. Brübach, B. Albert, A. Dreizler, Cylinder head temperature determination using high-speed phosphor thermometry in a fired internal combustion engine. *Appl. Phys. B* **116**(2), 293–303 (2014)
17. N. Fuhrmann, E. Baum, J. Brübach, A. Dreizler, High-speed phosphor thermometry. *Rev. Sci. Instrum.* **82**(10), 104903 (2011)
18. N. Fuhrmann, J. Brübach, A. Dreizler, Phosphor thermometry: a comparison of the luminescence lifetime and the intensity ratio approach. *Proc. Combust. Inst.* **34**(2), 3611–3618 (2013). <https://doi.org/10.1016/j.proci.2012.06.084>
19. S.W. Allison, G.T. Gillies, Remote thermometry with thermographic phosphors: instrumentation and applications. *Rev. Sci. Instrum.* **68**(7), 2615–2650 (1997)
20. A.H. Khalid, K. Kontis, Thermographic phosphors for high temperature measurements: principles, current state of the art and recent applications. *Sensors* **8**(9), 5673–5744 (2008)
21. J. Brübach, C. Pflitsch, A. Dreizler, B. Atakan, On surface temperature measurements with thermographic phosphors: a review. *Prog. Energy Combust. Sci.* **39**(1), 37–60 (2013)
22. K. Tsuchiya, K. Sako, N. Ishiwada, T. Yokomori, Precision evaluation of phosphors for the lifetime method in phosphor thermometry. *Meas. Sci. Technol.* **31**(6), 065005 (2020)
23. N.J. Neal, J. Jordan, D. Rothamer, Simultaneous measurements of in-cylinder temperature and velocity distribution in a small-bore diesel engine using thermographic phosphors. *SAE Int. J. Engines* **6**(2013-01-0562), 300–318 (2013)
24. J. Jordan, D. Rothamer, Pr:Yag temperature imaging in gas-phase flows. *Appl. Phys. B* **110**(3), 285–291 (2013). <https://doi.org/10.1007/s00340-012-5274-4>
25. D. Witkowski, D.A. Rothamer, Emission properties and temperature quenching mechanisms of rare-earth elements doped in garnet hosts. *J. Lumin.* **192**, 1250–1263 (2017)
26. N. Fuhrmann, M. Schild, D. Bensing, S.A. Kaiser, C. Schulz, J. Brübach, A. Dreizler, Two-dimensional cycle-resolved exhaust valve temperature measurements in an optically accessible internal combustion engine using thermographic phosphors. *Appl. Phys. B* **106**(4), 945–951 (2012)
27. S. Weisberg, *Applied Linear Regression*, vol. 528 (Wiley, New York, 2005)
28. J. Brübach, J. Janicka, A. Dreizler, An algorithm for the characterisation of multi-exponential decay curves. *Opt. Lasers Eng.* **47**(1), 75–79 (2009)
29. M.D. Dramićanin, B. Milićević, V. Orević, Z. Ristić, J. Zhou, D. Milivojević, J. Papan, M. G. Brik, C. Ma, A. M. Srivastava, Li₂tio₃: Mn⁴⁺ deep- red phosphor for the lifetime- based luminescence thermometry. *ChemistrySelect* **4**(24), 7067–7075 (2019)
30. J.D. Ingle, S.R. Crouch, Signal-to-noise ratio comparison of photomultipliers and phototubes. *Anal. Chem.* **43**(10), 1331–1334 (1971)